Electronic Supplementary Material (ESI) for Nanoscale.

Supporting Information

A Bifunctional Electrode Engineered by Sulfur Vacancies for Efficient Electrocatalysis

Fan Wang,[a] Kai Li,[a] Jingjing Li,[a] Lawrence M. Wolf,[b] Kai Liu,[a] Hongjie Zhang[a]*

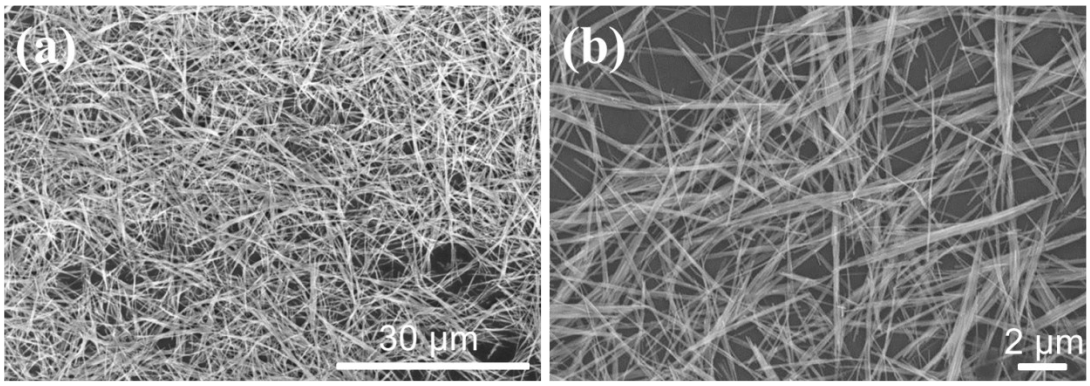

Figure S1. The SEM results reveal that the CdS NWs have highly uniform 1D morphology with mean diameter of 50nm and a length of several micrometers.

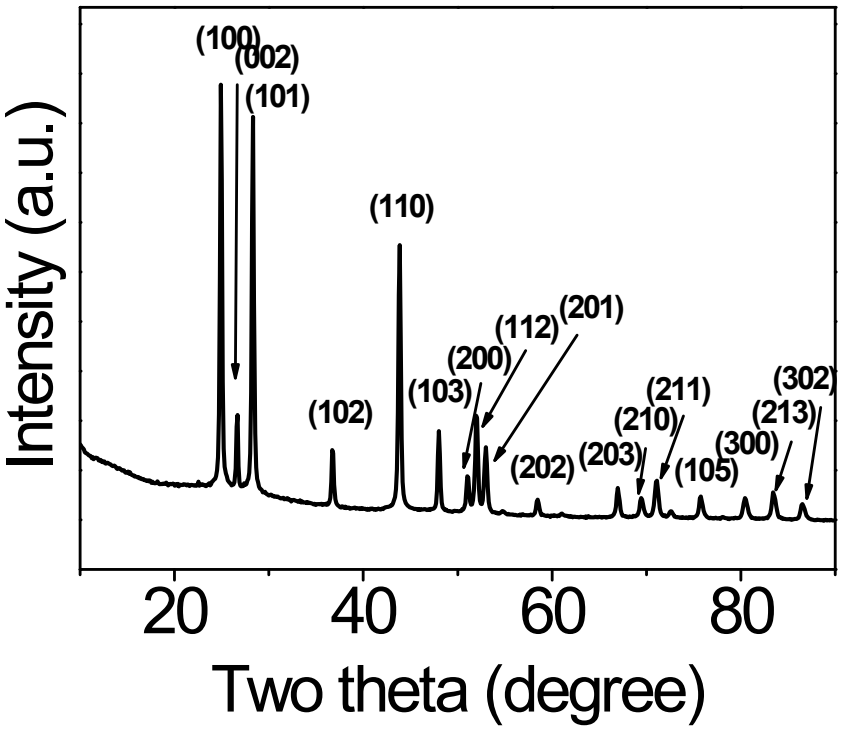

Figure S2. The XRD patterns of CdS NWs can be ascribed to the hexagonal phase of CdS NWs (JCPDS No. 41-1049).

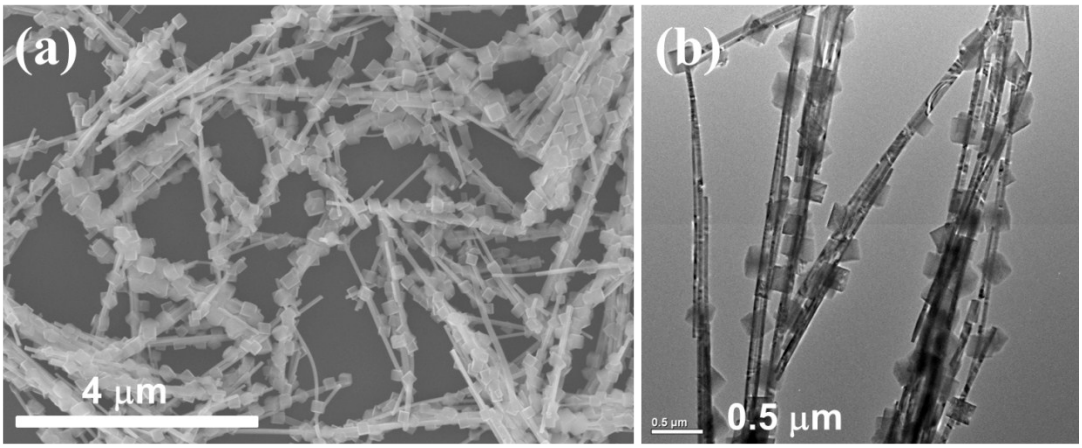

Figure S3. The SEM and TEM results of CdS@(Ni, Fe)-PBA. CdS NWs display obvious positively charged surface, thus CdS NWs can be used as templates to form hybrids with prussian blue analogue by adding Fe^{3+}, Ni^{2+}, and ligands. Uniform and monodisperse cubes with a structure of candied haws on a CdS stick are presented. The size of cube is about 200 nm.

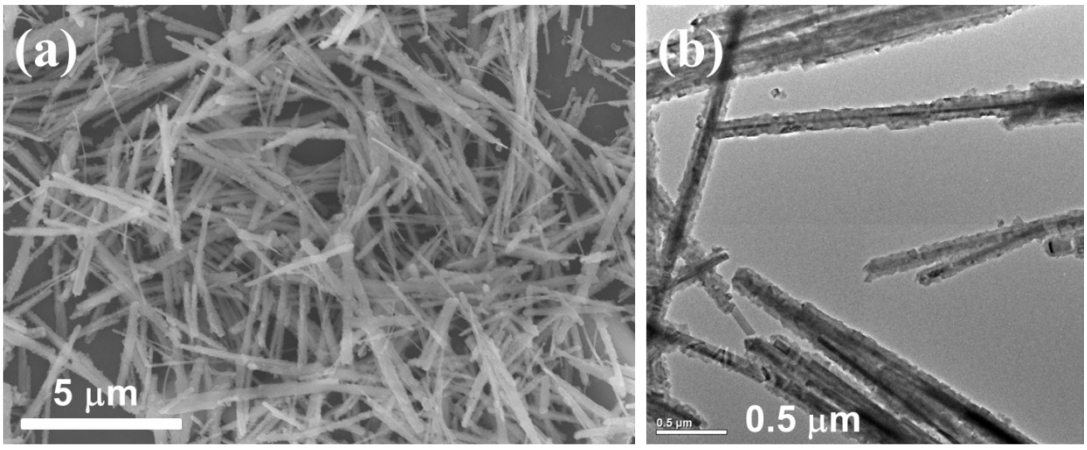

Figure S4. The SEM and TEM results of CdS@(Ni, Co, Fe)-PBA. Uniform and monodisperse core@shell structures are presented. The size of cube is about 50 nm.

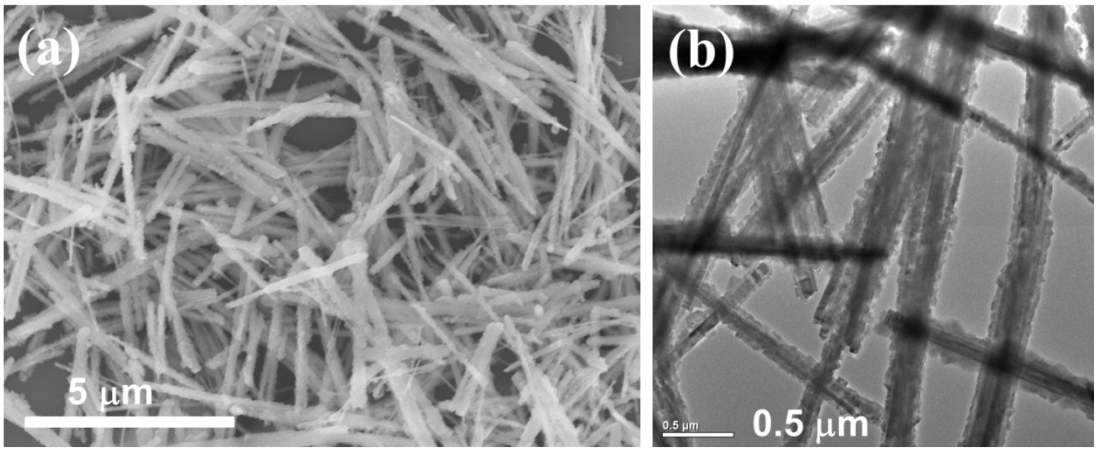

Figure S5. The SEM and TEM results of CdS@(Co, Fe)-PBA. The structure of CdS@(Co, Fe)-PBA is similar to that of CdS@(Ni, Co, Fe)-PBA. The size of cube is about 100 nm. Based on the SEM and TEM results of CdS@(Ni, Fe)-PBA, CdS@(Ni, Co, Fe)-PBA and CdS@(Co, Fe)-PBA, the size of cube might be manipulated by tuning the doping concentration of Ni^{2+} and Co^{3+}.

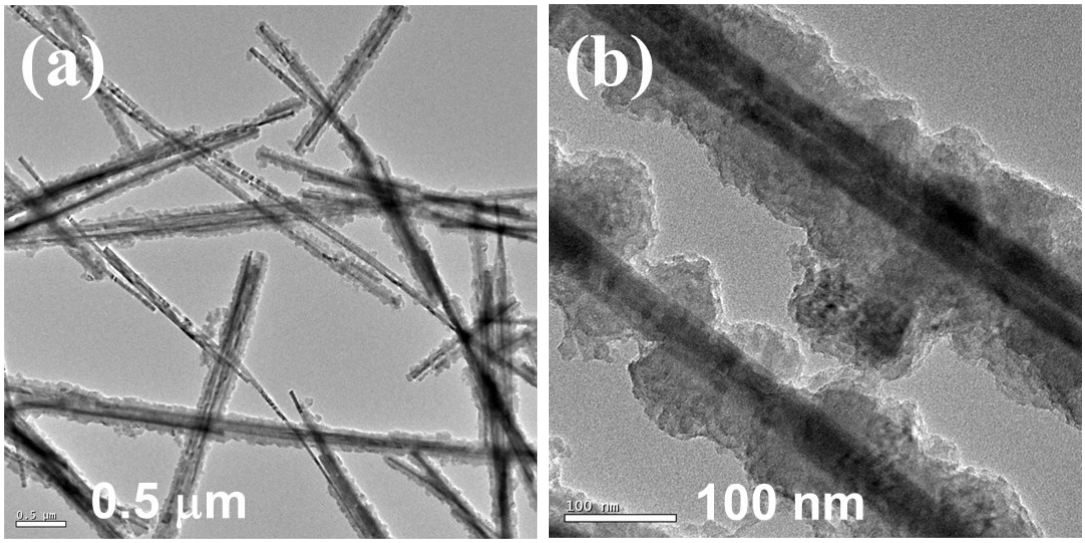

Figure S6. The TEM results of CdS@(Co, Fe)-PBA@PDA. The structure of CdS@(Co, Fe)-PBA@PDA is similar to that of CdS@(Ni, Co, Fe)-PBA@PDA except for the size of cubes. The uniform core@shell nanomaterials with a thickness of approximately 8.5 nm of PDA are presented.

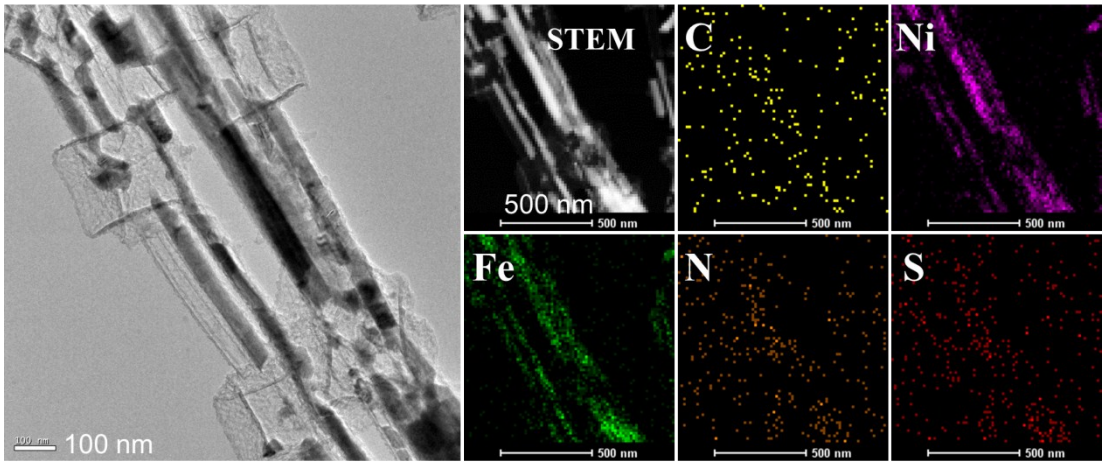

Figure S7. The TEM and STEM-EDS results of (Ni, $Fe)_9S_8$ embedded N-doped carbon. By sintering, the evaporation of Cd vapor accelerated the releasing of free S atoms, which led to the formation of (Ni, $Fe)_9S_8$ embedded N-doped carbon. The STEM-EDS results show that the sulfides are not only located in the carbon backbone, but also they are embedded in the cubes.

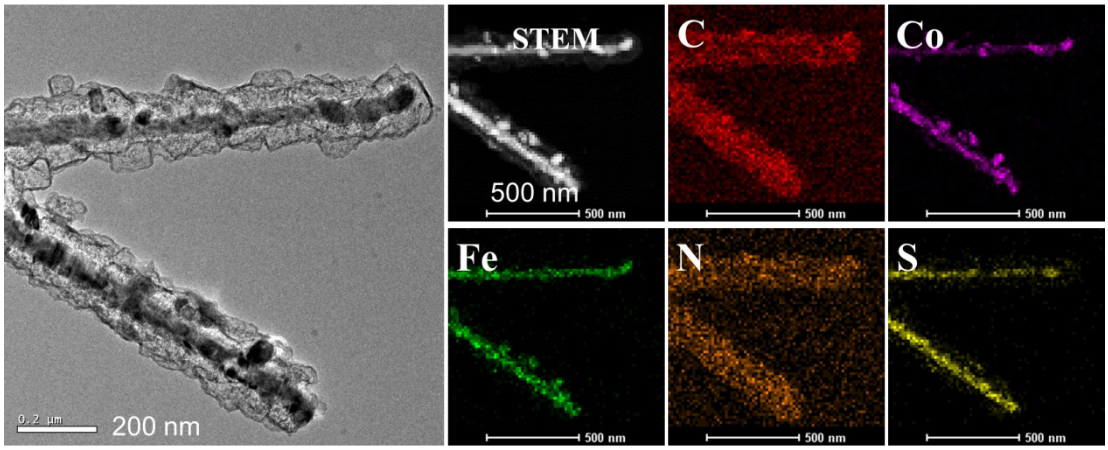

Figure S8. The TEM and STEM-EDS results of Co_8FeS_8 embedded N-doped carbon. By sintering, the evaporation of Cd vapor accelerated the releasing of free S atoms, which led to the formation of Co_8FeS_8 embedded N-doped carbon. The STEM-EDS results also show that the sulfides are not only located in the carbon backbone, but also they are embedded in the cubes.

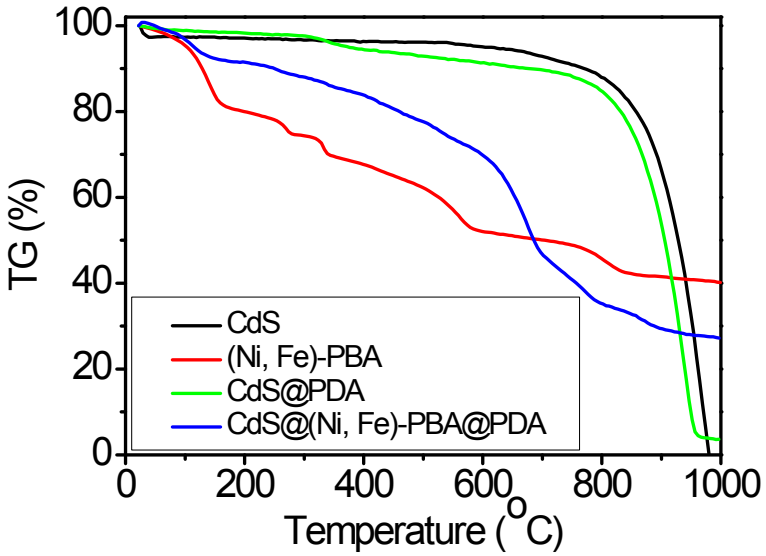

Figure S9. TGA curves of CdS, (Ni, Fe)-PBA, CdS@PDA and CdS@(Ni, Fe)-PBA@PDA. The TGA curves are used to illustrate the thermal behavior of CdS@(Ni, Fe)-PBA@PDA. Three stable intervals are obviously observed. A swift weight loss between 200 and 800 °C was detected, caused by the carbonization of the PDA and (Ni, Fe)-PBA. Another weight loss occurs with a further increase of temperature, which is attributed to the evaporation of Cd due to its low boiling point (765 °C). According to the TGA curves, the (Ni, $Fe)_9S_8$ embedded N-doped carbon content is calculated to be about 30 wt %.

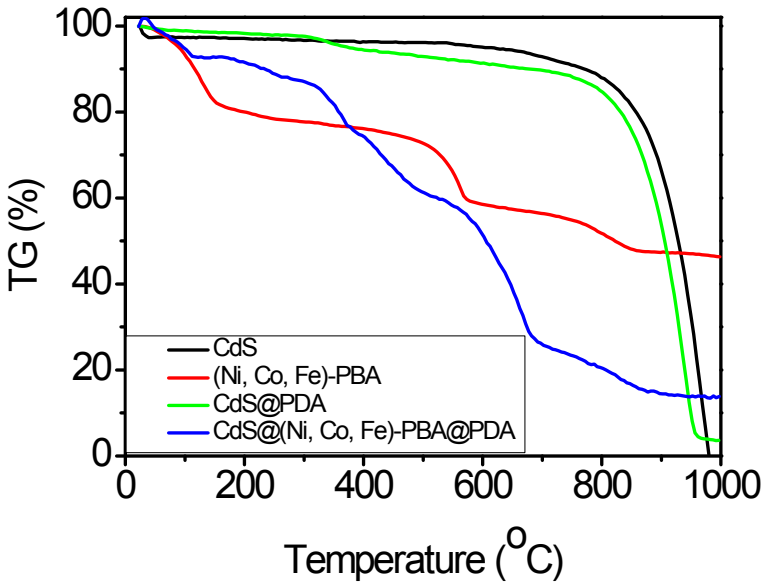

Figure S10. TGA curves of CdS, (Ni, Co, Fe)-PBA, CdS@PDA and CdS@(Ni, Co, Fe)-PBA@PDA. According to the TGA curves, the (Ni, Co, Fe)$_9$S$_8$ embedded N-doped carbon content is calculated to be about 13 wt %.

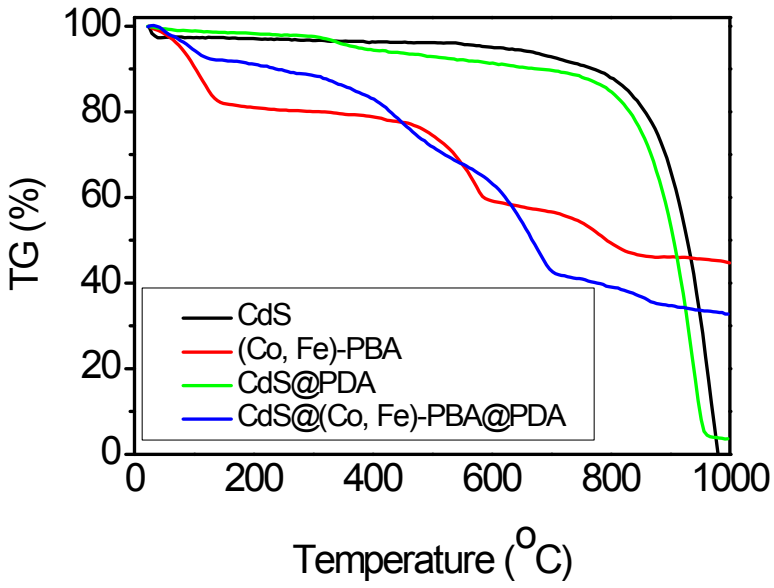

Figure S11. TGA curves of CdS, (Co, Fe)-PBA, CdS@PDA and CdS@(Co, Fe)-PBA@PDA. According to the TGA curves, the $(Co, Fe)_9S_8$ embedded N-doped carbon content is calculated to be about 33 wt %.

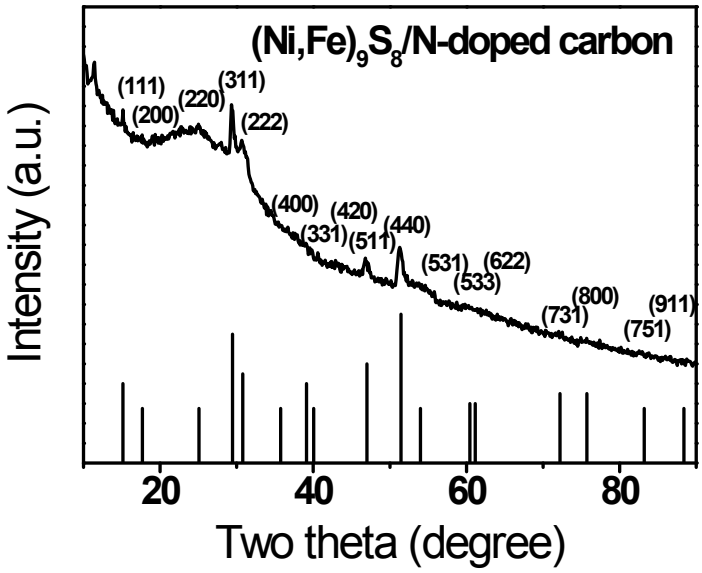

Figure S12. The results of XRD confirm the completely removal of CdS in (Ni, $Fe)_9S_8$/N-doped carbon. At approximately 2θ = 26 °, we observe a broad peak, which refers to the C (002). The results of XRD can be ascribed to the phase of (Ni, $Fe)_9S_8$ (JCPDS No. 08-0090).

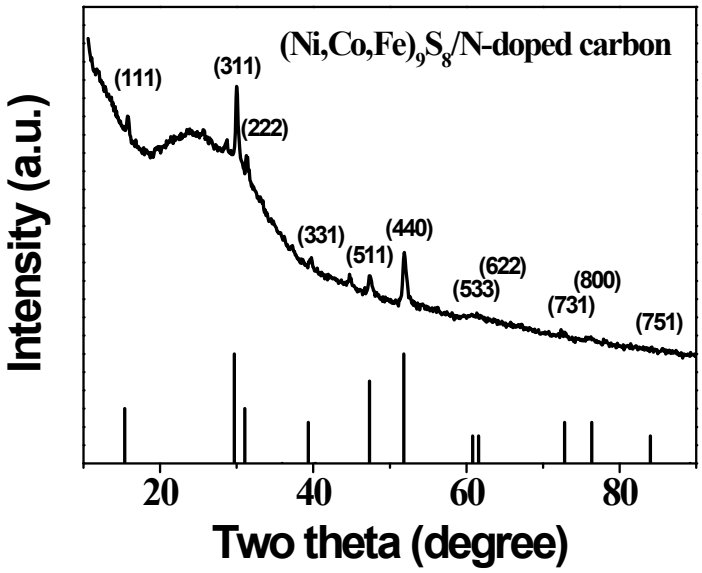

Figure S13. The results of XRD confirm the completely removal of CdS in (Ni, Co, Fe)$_9$S$_8$/N-doped carbon. The results of XRD can be ascribed to the phase of (Ni, Co, Fe)$_9$S$_8$ (JCPDS No. 19-0364).

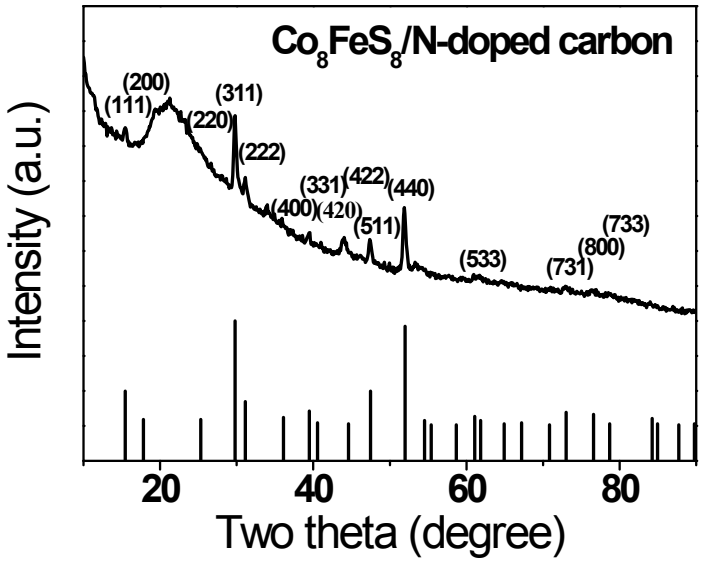

Figure S14. The results of XRD confirm the completely removal of CdS in Co_8 FeS_8/N-doped carbon. The results of XRD can be ascribed to the phase of Co_8 FeS_8 (JCPDS No. 29-0484).

Table S1. The results of ICP-MS confirm the completely removal of CdS in (Ni, $Fe)_9S_8$/N-doped carbon, (Ni, Co, $Fe)_9S_8$/N-doped carbon and Co_8 FeS_8/N-doped carbon. The ICP-MS analysis determines the Ni, Co, Fe contents. The molar ratio of Co/Fe equals to the ideal stoichiometric ratio of the structure of Co_8FeS_8.

Samples	Ni (ppm)	Co (ppm)	Fe (ppm)	Cd (ppm)	Ni/Co/Fe
$(Ni,Fe)_9S_8$/N-doped carbon	203700	0	141600	0	5/0/4
$(Ni,Co,Fe)_9S_8$/N-doped carbon	46190	88690	95230	0	1/2/2
Co_8FeS_8/N-doped carbon	0	191400	23879	0	0/8/1

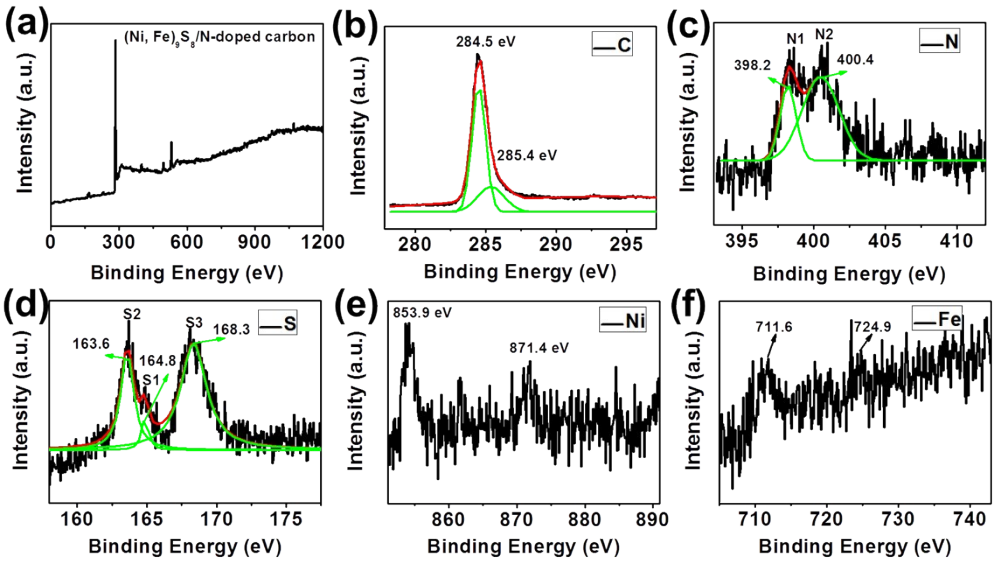

Figure S15. XPS spectra of (Ni, $Fe)_9S_8$/N-doped carbon. The C 1s spectra for (Ni, $Fe)_9S_8$/N-doped carbon can be divided into two major peaks corresponding to C-C (284.5 eV, C1), C=N (285.4 eV, C2), which further indicates that N has been successfully doped into the carbon nanomaterias. The N 1s spectrum can be mainly divided into two peaks with binding energies at 398.2 eV (pyridinicN, N1), 400.4 eV (pyrrolic–N, N2), while S 2p spectrum can be resolved into three different peaks at 163.6 eV (S2), 164.8 eV (S1) and 168.3eV, which could be attributed to $S2p_{3/2}$, $S2p_{1/2}$ peaks and -SO_x (x = 2-4).

x (x = 2−4), respectively. The Ni 2p region spectrum shows that the main peak at 853.9 eV with a satellite attributed to Ni $2p_{1/2}$ and the peak at 871.4 eV with a satellite attributed to Ni $2p_{3/2}$ are both characteristic of Ni^{2+}. The binding energy of Fe exhibits two main peaks at 711.6 and 724.9 eV, attributed to the $2p_{3/2}$ and $2p_{1/2}$.

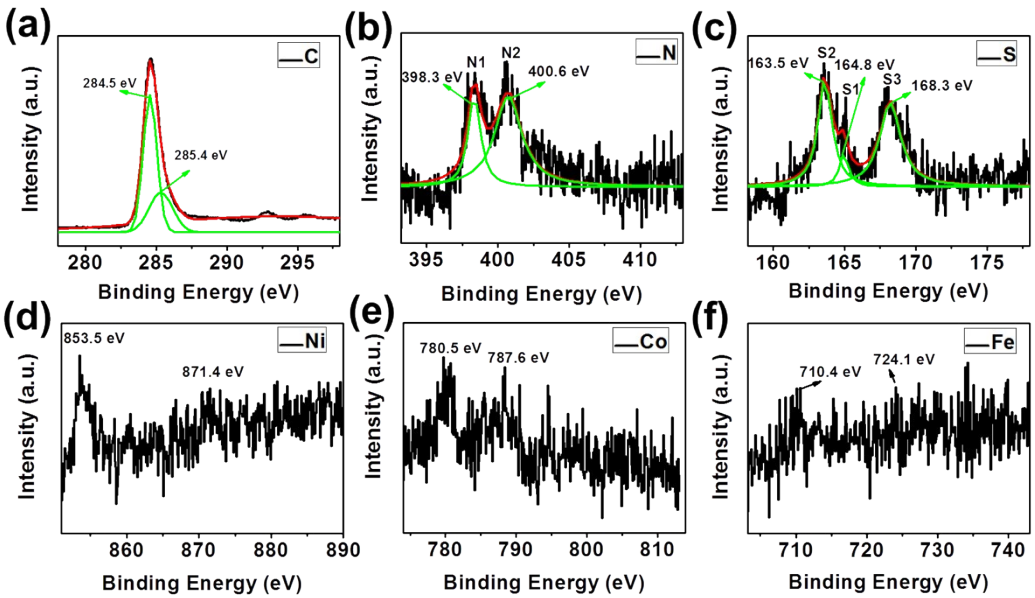

Figure S16. XPS spectra of (Ni, Co, Fe)$_9$S$_8$/N-doped carbon. The C 1s spectra also indicates that N has been successfully doped into the carbon nanomaterias. The N 1s, S 2p, Ni 2p and Fe 2p spectrum are similar with those of (Ni, Fe)$_9$S$_8$/N-doped carbon. The binding energy of Co exhibits two main peaks at 780.5 and 787.6 eV, attributed to the 2p$_{3/2}$ and 2p$_{1/2}$.

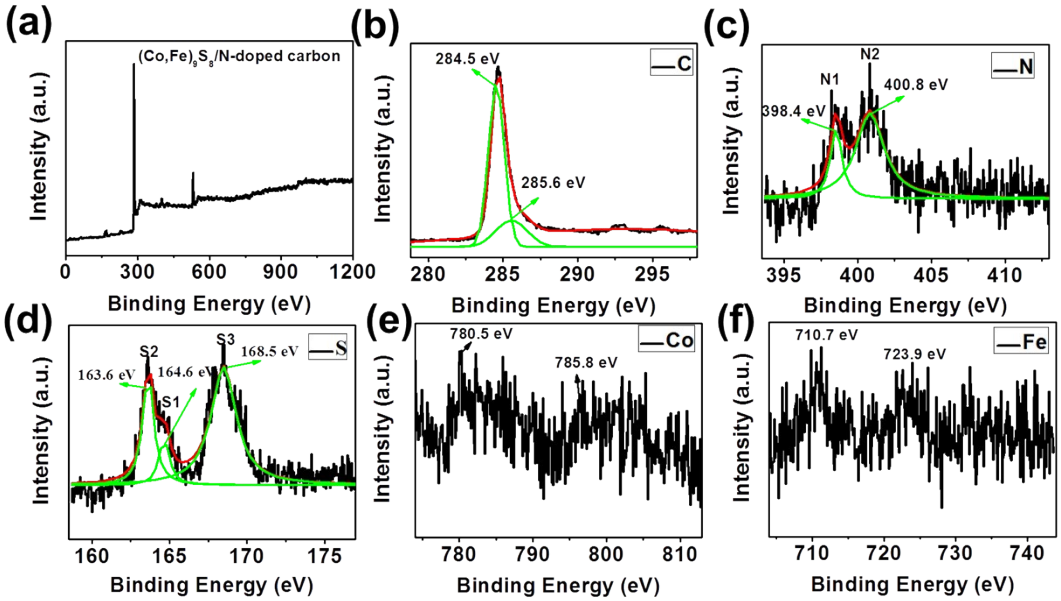

Figure S17. XPS spectra of Co_8FeS_8/N-doped carbon. The C 1s spectra indicates that N has been successfully doped into the carbon nanomaterias. The N 1s, S 2p, Co 2p and Fe 2p spectrum are similar with those of (Ni, Co, Fe)$_9S_8$/N-doped carbon.

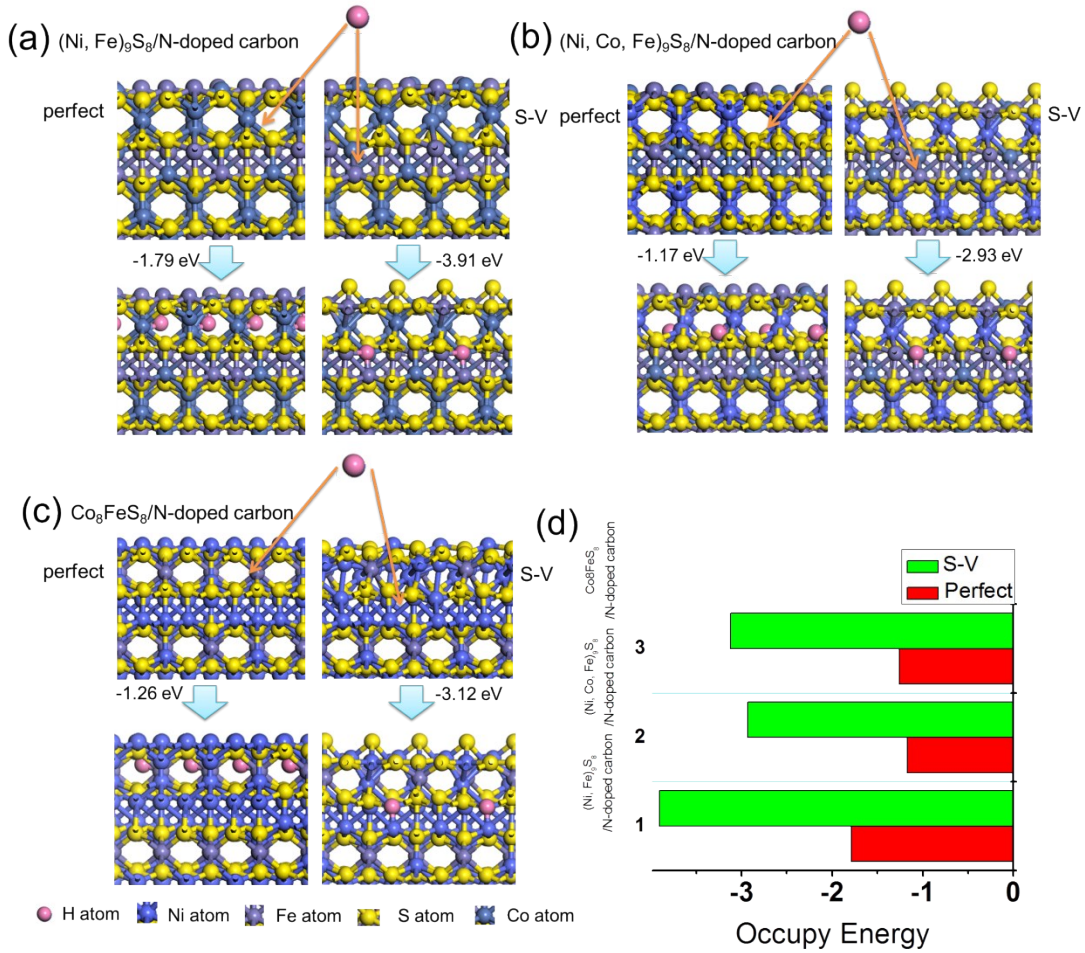

Figure S18. DFT simulation and occupy energy calculation of the prepared nanocatalysts. The structures of Ni-Co-Fe chalcogenides/nitrogen-doped carbon with sulfur vacancies (S-V) or without sulfur vacancies (perfect) were simplified with (111) plane based on the XRD, XPS and TEM results. The energy required for introducing H atoms at the interstitial position in above two situations, with and without sulfur vacancies, were calculated. The lower occupy energy (far away from zero) denotes stronger occupation. The three samples have the same trend in decreasing occupy energies with the formation of sulfur vacancies.